Research Signpost
37/661 (2), Fort P.O., Trivandrum-695 023, Kerala, India

Recent Developments in Vacuum Science and Technology, 2003: 111-132 ISBN: 81-7736-118-X
Editor: Jarek Dąbrowski

7 Hydrogen on palladium: A model system for the interaction of atoms and molecules with metal surfaces

Markus Lischka and Axel Groß
Physik-Department T30, Technische Universität München, D-85747 Garching, Germany

Abstract

The interaction of H with Pd surfaces has served as a model system in surface science. We review theoretical aspects of the adsorption and absorption phenomena that have been studied in this system. Issues such as the site dependence of atomic adsorption energies, lateral interactions between adsorbates, adsorption on stepped surfaces, poisoning of surface reactions, adsorbate induced reconstructions, coexistence of atomic and molecular species, and dynamics of adsorption and desorption are addressed. The results, which are mainly based on first-principles electronic structure theory, allow the identification of fundamental principles and mechanisms in the interaction of atoms and molecules with metal surfaces.

1. Introduction

The interaction of atoms and molecules with surfaces is of great technological relevance. The rate

Correspondence/Reprint request: Dr. Axel Groß, Physik-Department T30, Technische Universität München, D-85747Garching Germany. E-mail: agross@ph.tum.de

of chemical reactions can be tremendously increased by the presence of a catalytic surface. Semiconductor devices are built by deposition and growth processes in molecular beam epitaxy. On the other hand, the performance of catalysts can be poisoned by the presence of adsorbates, and corrosion decreases the durability of mechanical systems. Again, these harmful processes can be avoided by coating the surfaces with some suitable material.

Usually the processes occurring on realistic surfaces are rather complex. In the surface science approach one tries to understand the fundamental principles underlying the interaction of atoms and molecules with surfaces by studying relatively simple systems under well-defined microscopic conditions. The hope is that the information gained in these systems helps to understand the processes that are going on at surfaces in a much more complex environment.

In particular, the interaction of hydrogen with palladium surfaces has been studied in great detail, both experimentally as well as theoretically. These studies were motivated among other reasons by the fact that bulk Pd can absorb huge amounts of hydrogen thus making it a possible candidate for a hydrogen storage device in the context of the fuel cell technology. Besides, Pd is also used as a catalyst for hydrogenation and dehydrogenation reactions. Still hydrogen/palladium represents a system that can be handled without particular problems in experiments under ultra-high vacuum conditions. Furthermore, it is also well suited for a theoretical treatment with modern electronic structure methods. Hence there is a wealth of microscopic information which is well established and double-checked through the fruitful combination of state-of-the-art experiments with ab initio total-energy calculations and related simulations. The complexity of the surface studies is also increasing steadily, thus more and more closing the so-called structure and pressure gaps between surface science and the “real world”.

We will provide an overview over the theoretical studies devoted to the system hydrogen on palladium in the last decade. Due to the development of efficient algorithms and the increase in computer power it has become feasible to determine the total energies of surface structures and potential energy surfaces (PES) of reactions at surfaces in great detail from first principles. Almost all of the studies presented in this review are based on density functional theory (DFT) calculations. In addition to the total energies, DFT calculations provide information about the electronic structure of a particular configuration. This allows also to establish general concepts underlying the observed phenomena and to identify the electronic factors determining the configuration and reactivity of particular structures. Therefore, the knowledge gained is indeed not limited to this specific system, but is of general importance for our understanding of the interaction of atoms and molecules with surfaces.

We will address phenomena such as the dependence of atomic adsorption energies on the chemisorption site, lateral interactions between adsorbates, adsorption on stepped surfaces, poisoning of surface reactions, adsorbate induced reconstructions, coexistence of atomic and molecular species, and dynamics of scattering, adsorption and desorption. This long list confirms the role of H/Pd as a model system for our general understanding of the interaction of atoms and molecules with surfaces.

II. H on palladium

Before addressing the interaction of hydrogen with Pd surfaces, we will first briefly focus on the H-Pd gas phase chemistry. The electronic structure of the free Pd atom

corresponds to the closed-shell configuration $4d^{10}5s^0$. The open-shell configuration $4d^9 5s^1$ is 0.95 eV higher in energy [1]. Despite the closed-shell configuration of the free atom, Pd shows the reactivity characteristic for a transition metal where the *d*-band is not fully occupied.

The H-Pd gas-phase chemistry has been determined in quantum chemical studies using high-quality calculations on the CASSCF and MRSDCI levels [2, 3]. The PdH molecule has a binding energy of $D = 2.34$ eV with respect to the free Pd and H atoms and a bond length of $r_e = 1.545$ Å [3] (see Fig. 1).

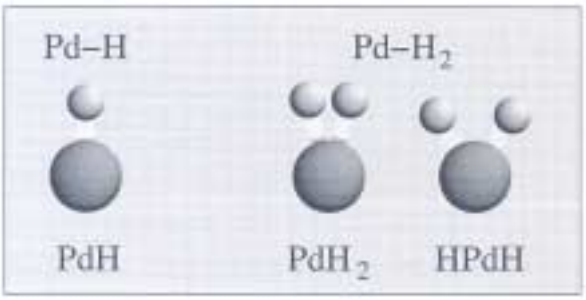

Figure 1. Structure of the PdH and PdH_2 molecules in the gas phase.

The palladium atom can also bind two hydrogen atoms in the gas phase, as illustrated in Fig. 1. There is a molecular dihydrogen complex of H_2 with an H-H bond length of $r_{H–H} = 0.864$ Å and Pd-H bond length of $r_{Pd–H} = 1.67$ Å [2]. There is a second metastable state that is 0.25 eV higher in energy which corresponds to the product of the oxidative addition. This H-Pd-H complex has a Pd-H bond length of $r_{Pd–H} = 1.50$ Å. It is only hindered by a small barrier for the reductive elimination back to the dihydrogen complex [1, 2]. The stable molecular configurations are also illustrated in Figure 1.

Unfortunately, the absolute binding energies of PdH_2 molecules have not been determined. It was deduced from the relative small change of the H-H bond length from the free H_2 molecule to the dihydride PdH_2 molecule that the interaction must be relatively weak and mainly mediated by van der Waals forces [2].

We will now turn to the interaction of hydrogen with palladium surfaces. Although bulk palladium can absorb large amounts of hydrogen, the most favorable position for hydrogen is *on* the surface, not in the bulk [4]. In Fig. 2 we have plotted the adsorption energy of atomic H on Pd(100) in the fourfold hollow and the bridge position as a function of the coverage determined by density functional theory calculations within the local density approximation (LDA) using the FP-LMTO method [4] and by DFT calculations employing the generalized gradient approximation (GGA) [6] for the exchange-correlation functional and using ultrasoft pseudotentials (US-PP) [5]. The coverage is defined as the number of hydrogen atoms per primitive surface unit cell.

Adsorption in the fourfold hollow position is much more favorable than at the bridge position. This is a general trend for hydrogen adsorption on low-index Pd surfaces: hydrogen generally prefers to adsorb at the highly coordinated sites [7]. As far as the lateral interactions between the adsorbates are concerned, the adsorption energy is only

weakly depending on the coverage in the fourfold hollow position. In fact, the adsorption energy is largest for $\theta = 0.5$ corresponding to a $c(2 \times 2)$ structure, and also the (1×1) hydrogen overlayer has a higher adsorption energy per hydrogen atom than the (2×2) structure.

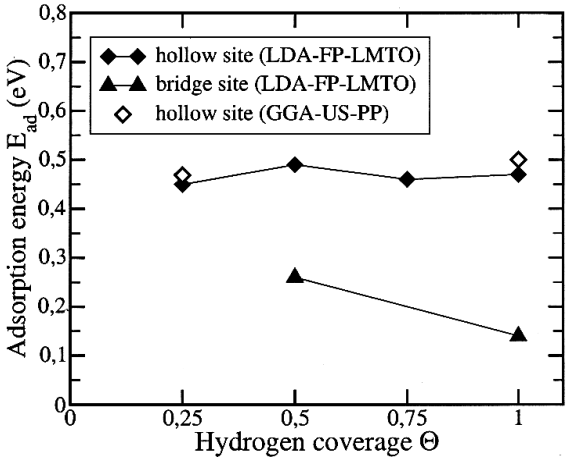

Figure 2. Coverage dependence of the adsorption energy of H/Pd(100) determined by LDA-FP-LMTO calculations [4] and by GGA-US-PP calculations [5]. The energies are referred to half of the binding energy of H_2 in the gas phase.

In contrast, on the bridge site the adsorption energy decreases with increasing coverage (Fig. 2) indicating a repulsive interaction between the H atoms. This repulsion can actually be traced back to the dipole-dipole interaction between adsorbed hydrogen atoms. On the bridge site the hydrogen atoms are located 1 Å above the surface layer (see Table 1). Due to a partial charge transfer from the surface there is a dipole moment associated with the hydrogen atoms. This is indeed confirmed by the calculated hydrogen-induced work function change of 390 meV which is also given in Table 1. The repulsive dipole-dipole interaction leads to the observed decrease in the adsorption energies for increasing coverage.

At the fourfold hollow site, on the other hand, the hydrogen atom is located at almost the same height as the surrounding Pd atoms. There is therefore almost no dipole moment associated with the hydrogen atoms which is reflected by the much lower work function change. The hydrogen atoms are effectively screened by the surrounding Pd atoms leading to a much smaller coverage dependence of the adsorption energy.

Table 1. Adsorption energies E_{ad}, adsorption heights h_0 and adsorbate-induced work function change $\Delta\Phi$ calculated for the adsorption of a (1×1) H monolayer on Pd(100) (from [8]).

Site	E_{ad} (eV)	(Å)	$\Delta\Phi$ (meV)
hollow	0.47	0.11	180
bridge	0.14	1.01	390

The fourfold hollow adsorption site on Pd(100) shows in fact an exceptional coverage dependence. This is demonstrated in Figure 3 where the atomic hydrogen adsorption energies for the most favorable adsorption sites on Pd(100) and Pd(111) [5], Pd(110)[9] and Pd(210) [10] determined by GGA-DFT calculations have been plotted as a function of the coverage. Note that since the coverage θ is related to the surface unit cells whose area is not the same for the different surfaces, the same coverage does not necessarily correspond to the same density. Still the general trend with the exception of Pd(100) is obvious: H atoms on the surface repel each other so that the H adsorption energy decreases for increasing coverage.

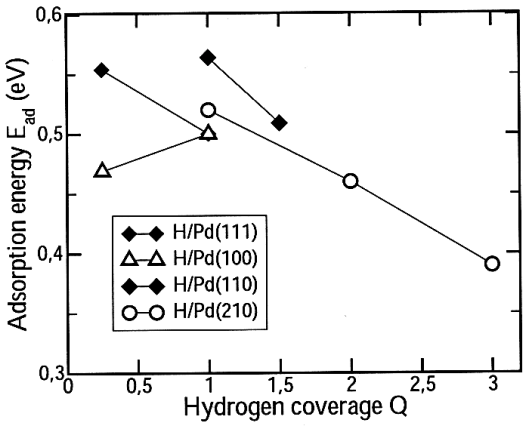

Figure 3. Coverage dependence of atomic hydrogen adsorption energies on various Pd surfaces determined by DFT calculations within the GGA. Pd(100) and Pd(111): Ref. [5], Pd(110): Ref. [9], Pd(210): Ref. [10].

This repulsion of adsorbed hydrogen atoms is most prominent on the Pd(210) surface where a saturation coverage of three hydrogen atoms per surface unit cell ($\theta = 3$) has been observed experimentally [11]. In Fig. 4, a top view of the Pd(210) surface including the atomic adsorption sites is plotted. As hydrogen adsorbs at high coordination sites on close-packed palladium surfaces, the species with the highest adsorption energy was tentatively assigned to the site with the highest coordination, i.e., the site labeled A in Fig. 4 with a four-fold coordination. The weaker bound H species were assigned to B and C', respectively (C' is actually twofold-degenerate due to the mirror symmetry along $[1\bar{2}0]$). As mentioned above, at the low-index Pd surface the energetic ordering of the atomic hydrogen adsorption sites indeed follows such a coordination argument.

In order to test this assumption for the Pd(210) surface, DFT adsorption energies at the three adsorption sites were computed in a (1×1) surface unit cell corresponding to a coverage of one monolayer. A comparison between theoretical adsorption energies and experimental ones derived from thermal desorption spectroscopy (TDS) [11] is shown in Table 2. It is found that the intuitive assignment based on local coordination is not valid on the (210) surface. Instead, the step site B is found to be the most attractive one. We

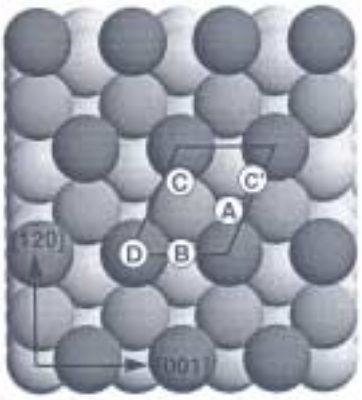

Figure 4. Top view of the (210) surface. In addition, the surface unit cell and the adsorption site labels are sketched.

Table 2. GGA-DFT adsorption energies per hydrogen atom on Pd(210) for different adsorption sites as a function of hydrogen coverage θ [10] compared to experimental results derived from thermal desorption spectroscopy [11]. For $\theta > 1$, the atomic adsorption energies are defined as the energies for additional adsorption of one H atom per surface unit cell with respect to the H_2 molecule in the gas phase. The notation of the sites refers to Fig. 4.

		E_{ad} [eV]	
Cov. θ	Site	Theory	Exp.
1	B	0.52	0.41
1	C'	0.51	
1	A	0.45	
2	B,A	0.40	0.33
3	B,A,C	0.26	0.23

note that site A, locally equivalent to a (100) hollow site, exhibits a very similar adsorption energy as reported for the (100) surfaces previously [7, 12].

If a monolayer of hydrogen is already adsorbed at site B, the next most favorable adsorption site at a $\theta = 2$ coverage is site A with a slightly decreased adsorption energy of E_{ad} = 0.40 eV compared to the pure surface. At an even higher coverage θ = 3, repulsive forces between the hydrogen atoms become dominant and the distance between the preadsorbed hydrogen atoms at site B as well as site A and the third hydrogen atom is maximized so that the third hydrogen atoms actually moves away from site C' to the bridge site C with a significantly reduced adsorption energy of E_{ad} = 0.26 eV. The results are summarized in Table 2 where the experimental TDS peaks [11] have been re-assigned according to the DFT adsorption energies.

The energetical ordering of the adsorption sites can be analyzed and understood in terms of their local reactivity. By projecting the Kohn-Sham wavefunctions to atomic orbitals (truncated to a sphere with radius r_s = 1.55 Å) [13], the layer-resolved local density of states (LDOS) as shown in Fig. 5 can be obtained. As proposed by Hammer and Nørskov [14, 15], the local reactivity is directly proportional to the distance of the

d-band center to the Fermi level. Within this model, the interaction energy is approximately given by the perturbation expression,

$$\Delta\varepsilon \sim \frac{V^2}{|\varepsilon_d - \varepsilon_{\mathrm{H}}|}, \quad V \ll |\varepsilon_d - \varepsilon_{\mathrm{H}}|. \tag{1}$$

Assuming a constant filling of the *d*-band and a constant coupling matrix V for different but similar configurations, it is only the distance $|\varepsilon_d - \varepsilon_{\mathrm{H}}|$ that determines the energy gain due to a bond formation.

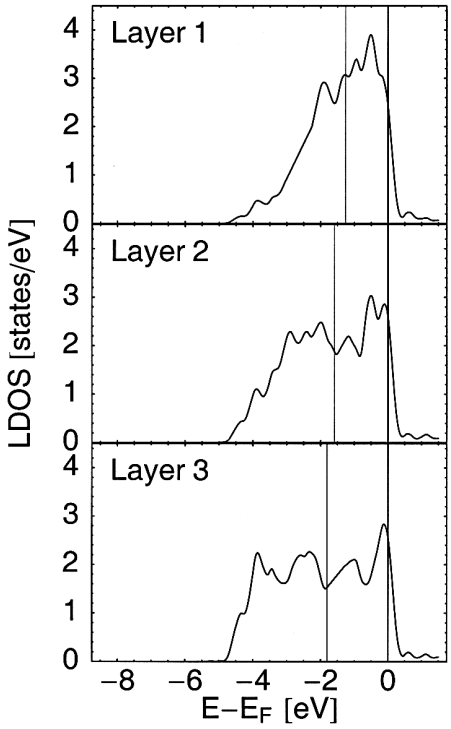

Figure 5. Layer-resolved, local *d*-band density of states. Indicated by vertical lines are the Fermi level and the center of the *d*-band. The third-layer LDOS is already very close to the bulk density of states of palladium [10].

For bulk Pd, the *d*-band center is located 1.86 eV below the Fermi level. Going from bulk to the surface, the *d*-band center moves gradually higher in energy towards the Fermi level, i.e., the *d*-band center of the third-layer atom is still close to the bulk value at $\varepsilon_d = -1.80$ eV whereas for the first-layer atom we obtain $\varepsilon_d = -1.26$ eV. According to the Hammer-Nørskov model, it is thus the top Pd atom that is by far the most reactive one. To estimate the chemisorption potential energies at the actual adsorption sites A, B and C', the geometrical average of the nearest neighbor *d*-band centers can be used [16].

This indeed predicts the right ordering of the adsorption sites. The major origin of the variations in the bonding strength can thus be attributed to the local variations of the electronic structure at the surface.

The described trend of the mutual repulsion of adsorbed hydrogen is also true for Pd(110). As far as the hydrogen adsorption on Pd(110) is concerned, another very interesting phenomenon occurs: adsorbate-induced reconstructions. Strongly interacting adsorbates like sulphur, oxygen, carbon and nitrogen can induce a restructuring of the surface [17]. As far as (110) metal surfaces are concerned, 5d fcc metal surfaces such as Au(110) or Pt(110) undergo a spontaneous reconstruction, whereas clean 3d and 4d metal surfaces such as Ni(110) and Pd(110) are stable in the unreconstructed (1×1) structure. However, already a relatively weakly chemisorbed species such as hydrogen induces a surface reconstruction of the Pd(110) surface. The hydrogen induced reconstruction is very sensitive to the hydrogen coverage. At coverages up to $\theta = 1$, unreconstructed Pd(110) surfaces have been found [18]. Experimentally, however, it is very hard to determine the positions of hydrogen atoms on the reconstructed surfaces because they hardly scatter electrons. Therefore hydrogen is almost invisible for experimental methods using electron diffraction techniques. This calls for theoretical support. And indeed, the hydrogen induced polymorphism has been studied in detail by DFT calculations [9, 19].

For one monolayer H on unreconstructed Pd(110), DFT calculations find that the (1×1) structure is not stable [9]. Hydrogen atoms adsorb rather in a (2×1) structure as illustrated in Fig. 6a which is more stable by 29 meV/atom. The driving force is again the dipole-dipole repulsion between the adsorbed hydrogen atoms. In the (2×1) structure consisting of zigzag chains of H atoms the distance between the hydrogen atoms on the surface is maximized. In addition, the hydrogen atoms are effectively screened by the Pd atoms in the top layer in this configuration which further reduces the repulsion. This (2×1) structure is indeed verified by the experiment [18].

Later experiments found that already at a hydrogen coverages at and below $\theta = 1$ adsorbate-induced reconstructions can occur [17]. Several different hydrogen adsorbate structures on reconstructed surfaces have been considered in the calculations. The most stable one for $\theta = 1$ is shown in Fig. 6b which is energetically more favorable by 62 meV/atom than the (2×1) superstructure on the unreconstructed surface. The structure corresponds to a missing-row reconstruction where every second row of Pd atoms on the (110) surface is missing. Upon this reconstruction, close-packed (111) facets are formed at the slopes of the V-shaped troughs. The particular hydrogen configuration maximizes the distance between the hydrogen atoms in the same trough thus minimizing their electrostatic repulsion.

Although this hydrogen-induced missing-row reconstruction is most stable, it is kinetically hindered which means that it is separated from the (2×1) superstructure by a sufficiently high energetic barrier. Hence the unreconstructed surface is metastable at low temperatures and only reconstructs when the temperature is increased [9].

Of course the question arises about the driving force that makes the missing-row reconstruction stable. The electronic structure calculations show that there is a general downshift of the energy levels upon hydrogen adsorption on the reconstructed surface compared to the unreconstructed surface. Thus it is an enhanced adsorbate-substrate interaction that stabilizes the missing-row reconstruction [9].

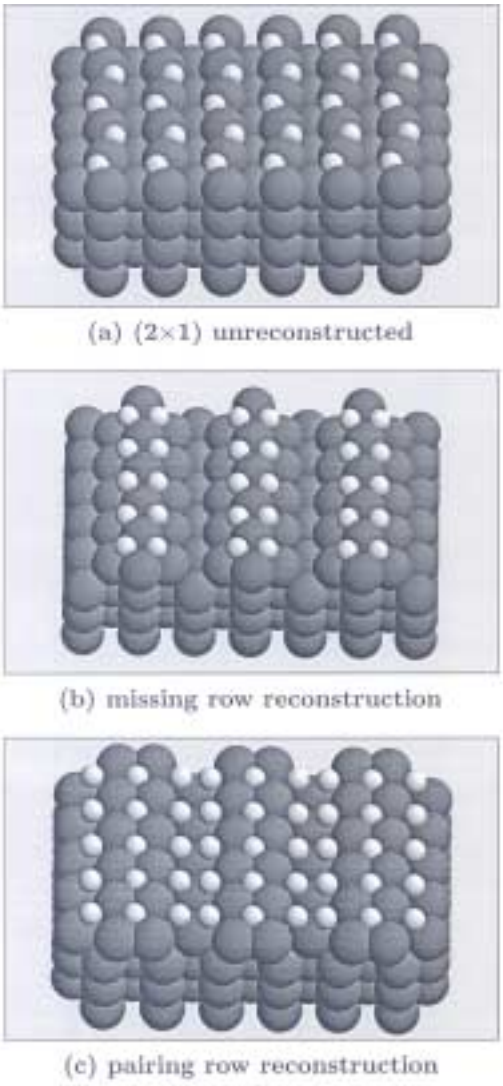

Figure 6. Hydrogen adsorption structures on Pd(110). (a) (2×1) unreconstructed surface for an hydrogen coverage of $\theta = 1$. (b) Hydrogen- induced missing-row reconstruction for $\theta = 1$. (c) Hydrogen-induced pairing-row reconstruction for $\theta = 1.5$ (after [9]).

Experimentally, a (1×2) pairing row reconstruction has also been observed [18]. Its structure is illustrated in Fig. 6c. It is obtained from the unreconstructed surface by pushing two adjacent Pd rows together. Furthermore, Fig. 6c illustrates the hydrogen adsorption pattern at a coverage of $\theta = 1.5$. There is also a stable pairing-row reconstruction for $\theta = 1$ which is equivalent to the structure for $\theta = 1.5$ with just the hydrogen atoms in the fourfold hollow positions between the paired rows missing.

However, at both coverages the pairing-row reconstruction is only meta-stable with respect to the missing-row reconstructions which are energetically still more favorable.

As far as the electronic structure of the H- covered Pd(110) surface in the pairing-row reconstruction is concerned, there is no indication of a significant downshift of the energy levels compared to the unreconstructed case. Hence electronic structure effects cannot be responsible for this reconstruction. An inspection of Fig. 6c shows that by pushing the Pd rows together, the H atoms in the threefold coordinated sites can increase their distance with respect to each other and thereby reduce their mutual repulsion. Hence the driving force for this reconstruction is mainly due to the electrostatic adsorbate-adsorbate repulsion.

So far we have focused on the hydrogen adsorption *on* the surface. However, as mentioned in the introduction, the interest in the H/Pd system was significantly motivated by the possibility to employ palladium as a hydrogen storage device. Hence, a number of theoretical studies have addressed the energetics of hydrogen absorption in subsurface layers [4, 20, 21, 22, 23, 7, 10]. In Fig. 7, the potential energy of a hydrogen atom above the fcc site of Pd(111) is plotted as a function of the distance from the surface. The energies have been determined by DFT-GGA calculations for a fixed substrate [20]. The first minimum corresponds to the adsorption *on* the surface, while the second minimum is due to hydrogen in the octahedral site in the first subsurface layer. One half of the H_2 dissociation energy is also indicated in Fig. 7, which determines the limit for stable adsorption. It is obvious that the subsurface site is energetically less favorable than the adsorption site on the surface. Therefore, for low coverages hydrogen will always stay on the surface and not penetrate into the bulk. If one doses palladium surfaces with more than one monolayer, then hydrogen will start to dissolve into the bulk [11].

As Fig. 7 demonstrates, subsurface hydrogen is even not stable with respect to the hydrogen molecule in the gas phase if the palladium crystal is not allowed to relax. This

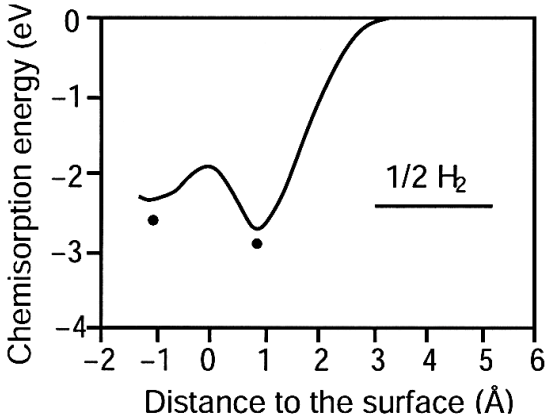

Figure 7. Potential energy of a H atom over a fcc hollow site of a Pd(111) surface as a function of the distance from the surface for a frozen substrate. The energies have been determined by DFT-GGA calculations [20]. The full line corresponds to a coverage of $\theta = 1$, while the filled circles denote a coverage of $\theta = 1/3$ (after [20]).

is caused by the fact that the lattice constant of PdH is larger by about 5 % than the Pd bulk lattice constant [22, 21]. If the surface is allowed to relax, then subsurface hydrogen becomes stabilized. In Table 3 we have collected the absorption energies and the top-layer relaxation in percent of the bulk layer spacing for atomic hydrogen in subsurface sites of various Pd surfaces calculated by DFT methods [4, 7, 10].

Table 3. Calculated values of the absorption energies and of the top-layer relaxation in percent of the bulk layer spacing for atomic hydrogen in subsurface sites of various Pd surfaces.

Surface	(111)	(100)		(110)	(210)	
Site	O_h	O_h	T_d	O_h	O_h	T_d
Energy (eV)	0.19[a]	0.18[a]	-0.06[b]	0.20[a]	0.21[c]	0.15[c]
Top-layer relaxation (%)	7.0[a]	8.8[a]	10.4[b]	5.1[a]	(-8.0[c])	–

[a] Ref. [7], [b] Ref. [4], [c] Ref. [10]

There are two different subsurface interstitial positions with either octahedral (O_h) or tetrahedral (T_d) symmetry. Atomic absorption in the octahedral site is energetically more favorable than in the tetrahedral because of the larger size of the octahedral gap. In fact, the absorption energy for subsurface hydrogen in the octahedral site is almost independent of the surface orientation showing that the binding properties of subsurface hydrogen are of local nature. The absorption energies in the subsurface position are still slightly larger than for interstitial bulk positions [21] so that hydrogen atoms in equilibrium will stay in near-surface regions. The occupation of the subsurface sites by hydrogen leads to a significant outward relaxation of the uppermost palladium layer. It is worthwhile noting that on the clean (210) surface the uppermost Pd layer already shows an inward relaxation of −17 % due to its open structure which is reduced −8 % by the presence of half a monolayer of hydrogen in the octahedral subsurface site [10] and finally completely vanishes for a full monolayer of subsurface hydrogen.

Figure 7 shows that the barrier for the absorption of hydrogen into the subsurface sites of Pd(111) is of the order of 0.8 eV per H atom with respect to the chemisorption minimum on the surface for unrelaxed Pd(111). This barrier, however, depends strongly on the distance and relaxation between the surface atoms [20]. If a hydrogen adlayer is already present on the surface, then the absorption of additional hydrogen into the surface site occurs via a concerted mechanism. The additional hydrogen adsorbs on the surface and pushes the underlying hydrogen atom to the subsurface site [21]. The barrier for this process is about 0.4 eV.

Based on experimental results it was proposed that hydrogen could directly absorb into the palladium bulk without equilibrating at the surface [24]. This motivated theoretical studies of direct subsurface adsorption of H_2 on Pd(111). The minimum barrier for the direct penetration corresponds to a configuration in which two hydrogen atoms cross the first palladium layer at adjacent fcc and hcp sites. The barrier for this process is still rather high for an unrelaxed substrate, the barrier height being 0.9 eV per H_2 molecule with respect to gas phase H_2 [22]. However, this barrier is also strongly influenced by surface relaxations. In a dynamical simulation, the onset energy for direct subsurface absorption was shifted down to 0.4 eV upon the inclusion of palladium surface motion [23].

III. H_2 on palladium

Usually hydrogen molecules adsorb dissociatively on metal surfaces [25]. In order to determine whether the dissociation of H_2 on Pd is activated or non-activated, the potential energy surface (PES) of the H_2 molecule approaching the Pd surface has to be determined. In Fig. 8 two contour plots along two-dimensional cuts through the six-dimensional coordinate space of H_2/Pd(100), so-called elbow plots, determined by GGA calculations [8] are shown. The coordinates in the figure are the H_2 center-of-mass distance from the surface z and the H-H interatomic distance d. The lateral H_2 center-of-mass coordinates in the surface unit cell and the orientation of the molecular axis, i.e., the coordinates x, y, θ, and ϕ are kept fixed for each 2D cut and depicted in the insets.

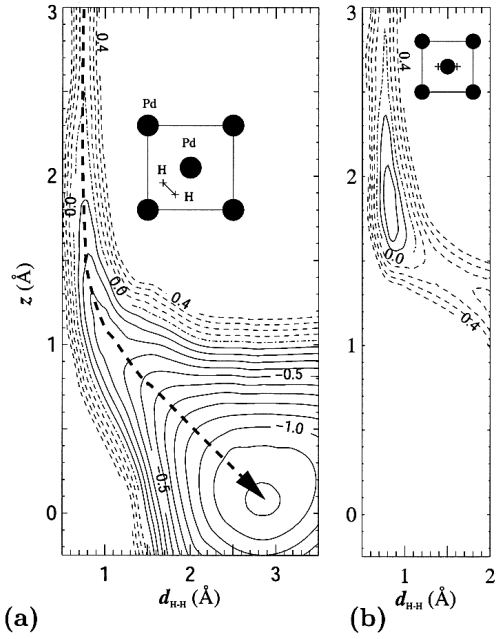

Figure 8. Contour plots of the PES along two two-dimensional cuts through the six-dimensional coordinate space of H_2/Pd (100) (from [8]). The contour spacing is 0.1 eV per H_2 molecule.

When the H_2 molecules approaches the Pd(100) surface with its center of mass above the bridge site and the H atoms pointing towards the four-fold hollow sites, the molecule can dissociate spontaneously without any hindering barrier. However, dissociative adsorption corresponds to a bond making-bond breaking process that depends sensitively on the local chemical environment. Indeed, if the molecules comes down over the on-top site, the shape of the PES looks entirely different. First the molecule is attracted towards the surface, in fact even more than above the bridge site, but then it encounters a barrier of more than 0.15 eV towards dissociation. The minimum in Fig. 8b is closely related to the molecular dihydride PdH_2 configuration. It does not, however, correspond to a local minimum but rather to a saddle point in the multi-dimensional PES. The H_2 molecule can

still move further downhill in the energy landscape if the center of mass of the H_2 molecule moves laterally away from the on-top position [12].

The PES does not only depend on the lateral position of the H_2 molecule, i.e., the PES is not only corrugated, but it is also strongly anisotropic. Only molecules with their axis parallel to the surface can dissociate, for molecules approaching the Pd surface in an upright orientation the PES is purely repulsive [8]. For H_2 adsorption on Pd(111) and Pd(110) the potential energy surfaces look similar [26, 27].

Under realistic conditions, surfaces are usually not clean but covered by adsorbates. Therefore the modification of the reactivity of a surface structure by the presence of adsorbates is of great technological relevance, especially in heterogeneous catalysis. Moreover, this modification is also interesting from a fundamental point of view since it allows to establish and verify reactivity concepts. Adsorbates can either promote or poison a particular reaction on the surfaces. The most prominent example for the reduction of the activity is the poisoning of the platinum-based car-exhaust catalyst by lead present in the gasoline. But not only lead, also sulfur causes a reduction of the efficiency of the car-exhaust catalyst.

In fact, the poisoning effect of sulfur is not restricted to oxidation reactions on platinum surfaces. On Pd(100), sulfur adsorption leads to a significant reduction of the hydrogen dissociation probability [29, 30]. In order to examine the microscopic effects of sulfur preadsorption, the potential energy surface of the H_2 dissociation on the $p(2 \times 2)$ and $c(2 \times 2)$ sulfurcovered Pd(100) surface has been determined in great detail by DFT studies [31, 28]. On $p(2 \times 2)$/Pd(100), H_2 dissociation is no longer non-activated as on the clean Pd(100) surface but hindered by a barrier of 0.1 eV. The closer the hydrogen molecules comes to the adsorbed sulfur atoms, the higher the barriers are for hydrogen dissociation indicating a strong repulsion between the adsorbed sulfur and H_2. On the $c(2 \times 2)$ sulfur-covered Pd(100) surface, the density of sulfur atoms is so high that the H_2 dissociation is effectively blocked by dissociation barriers larger than 2 eV [28].

The electronic factors influencing the reactivity of the sulfur-covered Pd(100) surface have been determined in detail by analyzing the local density of state of the interacting system. In Fig. 9, the density of states (DOS) projected onto the hydrogen, sulfur and palladium atoms is plotted for three different configurations. Fig. 9a corresponds to the non-interacting system with the hydrogen molecule still far away

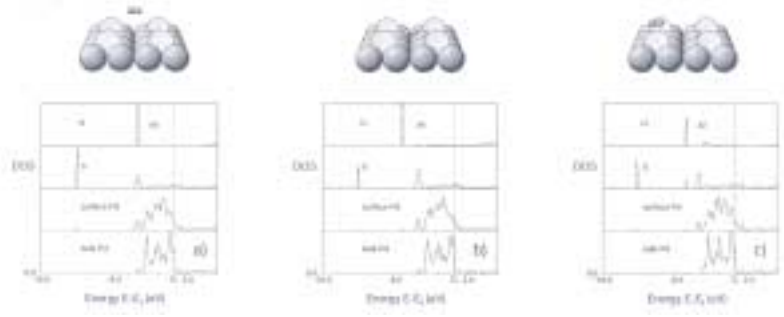

Figure 9. Local density of states for three different configurations in the hydrogen dissociation process on (2×2) sulfur-covered Pd(100). The upper panels indicate the corresponding position of the hydrogen molecule (after [28]).

from the surface. The prominent peak in the hydrogen DOS is given by the bonding σ_g state. It seems to be in resonance with a sulfur-related state but this is just coincidental. This is confirmed by Fig. 9b, which corresponds to the configuration at the minimum barrier for dissociation. The hydrogen and sulfur-related states are no longer in resonance indicating that there is no direct interaction between H_2 and the sulfur atoms for this configuration. In fact, it turns out that the building up of the minimum barrier is an indirect effect of the sulfur adsorption [28]: sulfur adsorption leads to a down-shift of the Pd *d*-states at the surface atoms which makes the surface more repulsive with respect to hydrogen dissociation [14, 15]. On the other hand, when the H_2 molecule directly approaches a sulfur atom (Fig. 9c), there is a strong hybridization and splitting in bonding and anti-bonding states between the H_2 and sulfur orbitals. Since both the bonding and anti-bonding contribution are fully occupied, the interaction is strongly repulsive [14].

As already mentioned, molecular hydrogen adsorption is usually not observed on transition metal surfaces. Only at very low temperatures below 20 K, very weakly bound molecular adsorption states can be trapped in shallow physisorption wells [32, 33]. The rare reports of molecular chemisorption of H_2, on the other hand, are restricted to stepped surfaces: The Pd(210) surface is such a surface that allows for a coexistence of atomic and molecular chemisorbed states.

By dosing the Pd(210) surface with H_2 at temperatures below 100 K, it was found in a series of thermal desorption experiments [11, 34] that not only three atomic adsorption states were populated, but also two distinct molecular adsorption states at desorption energies of 155 meV and 250 meV. Nevertheless, DFT calculations for the H_2 adsorption process on the pure Pd(210) surface revealed a scenario very similar to the H_2/Pd(100) system as illustrated in Fig. 8. The dissociation of an H_2 molecule into the hollow positions of the terrace or the "truncated" hollow positions at the steps is non-activated and molecular states should thus not exist. On the other hand, pre-adsorption of another species often leads to an increase of dissociation barriers effectively blocking any further atomic adsorption. In the case of Pd(210), hydrogen itself can effectively poison the surface so that a molecular adsorption state gets stabilized. As shown in Fig. 10a, the straight dissociation of molecular hydrogen is blocked by an activation barrier

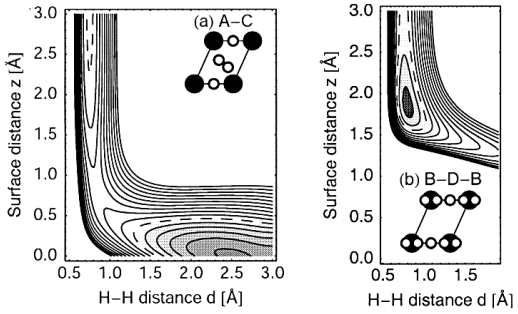

Figure 10. Two-dimensional sections through the PES for the dissociative adsorption of H_2 on Pd(210) precovered with a monolayer of hydrogen (θ=1). The molecular orientation is indicated in the insets. The contour spacing is 0.1 eV, and the vacuum energy level is marked by the dashed contour line.

once a monolayer of atomic hydrogen is already present on the surface. The adsorption well over the on-top site (Fig. 10), on the other hand, corresponds to a true minimum of the full PES now and, although its depth is slightly reduced, it is still reactive enough to trap an H_2 molecule with an adsorption energy of 0.27 eV [10].

Molecular adsorption of H_2 on Pd(210) is thus governed by the following scenario of local self-poisoning: On clean Pd(210), hydrogen dissociates and adsorbs. Once atomic hydrogen is present on the Pd(210) surface, any further hydrogen dissociation is kinetically hindered close to the adsorbed hydrogen atoms although atomic adsorption sites are still available. This situation is depicted in Fig. 11: A monolayer of atomic hydrogen (shown in white) is already adsorbed in the most favorable adsorption sites interspersed between the dark top-layer Pd atoms. Molecular hydrogen is then trapped over the top-layer Pd atom right at the steps. The hybridization of the molecule with the

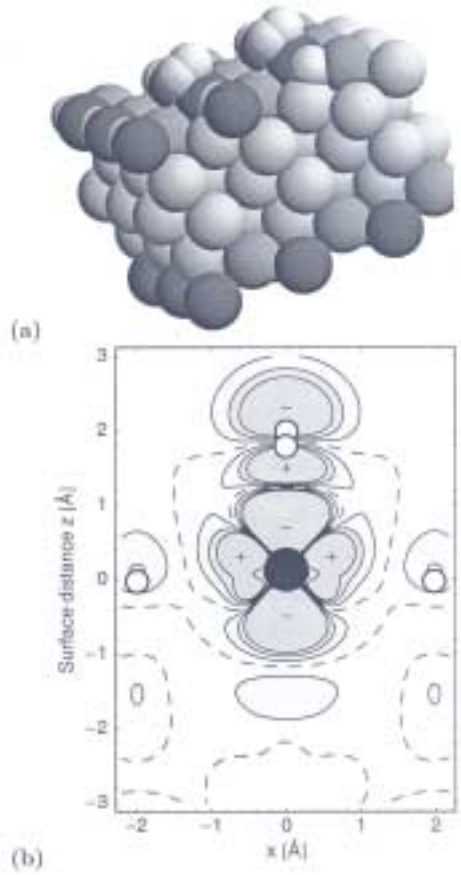

Figure 11. (a) Side view of the Pd(210) surface with a monolayer H precoverage and the molecular precursor. (b) Electron-density difference plot of the molecular adsorption state in the plane of the atomic hydrogen row and the surface normal. The positions of the H atoms and the top Pd atom are marked by open and filled circles, respectively.

Pd *d*-states and its strong polarization are clearly visible in the charge density difference plot of Fig. 11b. Regions of reduced electronic density (i.e., positively charged) compared to the isolated systems H_2 and H/Pd(210) are marked with a minus sign, regions of enhanced electron density with a plus sign. There is a strong charge rearrangement upon the H_2 adsorption on the hydrogen-covered Pd(210) surface. The polarization of the adsorbed H_2 molecule also leads to a large decrease of the work function which is confirmed by experiment [34]. It is worthwhile pointing out that the second molecular species found in the experiments is then attributed to a local atomic precoverage of $\theta = 2$ within this scenario and not to a different geometrical adsorption site.

It is only through its specific structure, i.e., its open steps and rather protrusive and reactive top-layer Pd atoms, that Pd(210) is capable of supporting both atomic and molecular adsorption states.

IV. Dissociation dynamics

The system H_2/Pd has served as the benchmark system for the non-activated dissociative adsorption on surfaces. Figure 12 compares the sticking probability for H_2/Pd(100) as a function of the kinetic energy obtained by molecular beam experiments [29] with the results of six-dimensional quantum calculations based on *ab initio* potential energy surfaces [35, 36]. The experiment shows an initial decrease of the sticking probability as a function of the kinetic energy while at larger kinetic energies the sticking probability slowly rises again.

The decrease of the sticking probability is typical for atomic or molecular adsorption where the molecule adsorbs non-dissociatively. Consequently, it was assumed that the hydrogen molecules do not directly dissociate on Pd(100). They are rather first trapped in a molecular precursor from which they then dissociate [29, 37], and it is the trapping probability into the precursor state that determines the dependence of the sticking probability on the kinetic energy.

However, there is a large mass mismatch between the impinging hydrogen molecule and the palladium substrate. Simple estimates show that the hydrogen molecules do not transfer enough energy to the substrate in order to become trapped at energies above 0.1 eV. Furthermore, the calculated potential energy surface shows no evidence of a metastable precursor state of H_2 at Pd(100). Still the quantum results of the sticking probability [35] are in semi-quantitative agreement with the experiment. As the inset of Fig. 12 demonstrates, with an improved potential energy surface based on more *ab initio* points even quantitative agreement with the experiment can be achieved [36].

The reason for the initially decreasing sticking probability is a dynamical process which had been proposed before [38] but whose efficiency had been grossly underestimated: dynamical steering. This process can only be understood if one takes into account the multidimensionality of the PES. The PES of H_2/Pd(100) shows purely attractive paths to-wards dissociative adsorption, but the majority of reaction paths for different molecular orientations and impact points exhibits energetic barriers hindering the dissociation.

At very low kinetic energies the particles are so slow that they can be very efficiently steered to a favorable configuration for dissociation. This leads to a very high dissociation probability. Since this mechanism becomes less effective at higher kinetic

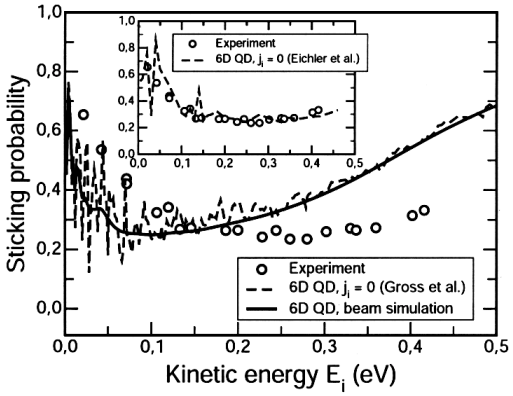

Figure 12. Sticking probability of H_2/Pd(100) as a function of the initial kinetic energy. Circles: experiment [29], dashed and solid line: theory according to H_2 initially in the ground state and with a thermal distribution appropriate for a molecular beam [35]. The inset shows the theoretical results using an improved *ab initio* potential energy surface [36].

energies, the reaction probability decreases. This scenario is illustrated in Fig. 13. A cut through the six-dimensional potential energy surface of H_2/Pd(100) is plotted along the reaction path coordinate and one surface coordinate. The reaction path coordinate connects the molecule in the gas phase with the dissociated molecule on the surface. There is one purely attractive path in the center which corresponds to the dissociation at the hollow-bridge-hollow configuration indicated in Fig. 8a while the path directly over the maximum barrier in Fig. 13 represents the dissociation above the top site (Fig. 8b).

Three typical trajectories are included in Fig. 13. The low and medium energy trajectories are related to each other by the mirror symmetry along the surface coordinate. They are supposed to have the same initial conditions except for the initial

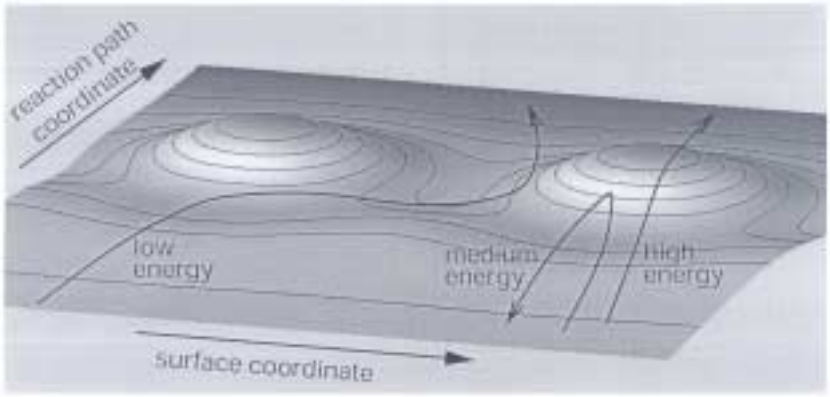

Figure 13. Illustration of the steering effect on a potential energy surface with a coexistence of purely attractive and repulsive paths towards dissociative adsorption. Three typical trajectories corresponding to the low, medium and high kinetic energy regime are included.

kinetic energy. Both energies are too small to allow a direct crossing of the barrier the particles are directed at. However, at the low kinetic energy the forces acting on the incoming particle can redirect it so that it follows a path that leads to the purely attractive region of the PES. At the medium energy, of course the same forces act on the incoming particle. But now it is too fast to be steered significantly. It is reflected at the repulsive part of the potential and scattered back into the gas phase. This suppression of the steering effect for increasing kinetic energy leads to the initial decrease of the sticking probability in Fig. 12. If the energy is further increased, then the particles will eventually have enough kinetic energy to directly cross barriers, as the high-energy trajectory illustrates in Fig. 13. This leads to the rise of the sticking probability at high kinetic energies.

This steering effect is strongly suppressed if the impinging molecules are rapidly rotating because molecules with a high angular momentum will rotate out of a favorable orientation towards dissociative adsorption during the time it takes to break the molecular bond. The dependence of the sticking probability on the initial rotational state was proposed as a property that can be used to distinguish between the steering and the precursor mechanism [39]. Molecular adsorption into a weak precursor state should be relatively independent of the rotational motion. This rotational hindering of the steering effect has actually been confirmed for H_2/Pd(111) [40, 41]. By seeding techniques the translational energy of a H_2 beam has been changed in a nozzle experiment without altering the rotational population of the beam. The rotationally hot beams showed a much smaller sticking probability than rotationally cold beams [40, 41].

The influence of internal molecular degrees of freedom on the dissociation process can also be probed by studying the time-reversed process of dissociative adsorption, associative desorption. In Fig. 14, so-called rotational temperatures in desorption are plotted. They correspond to the mean rotational energy in desorption via $T_{\mathrm{rot}} = \langle E_{\mathrm{rot}} \rangle / k_B$. According to the principle of detailed balance, the suppression of the sticking probability by the rotational hindering should be reflected by a population of rotational excited states in desorption which is lower than expected for molecules in thermal equilibrium

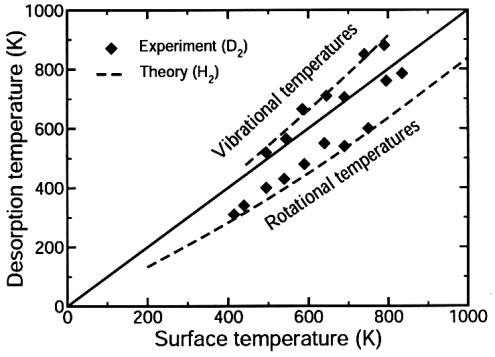

Figure 14. Vibrational and rotational temperatures of hydrogen desorbing from Pd(100) as a function of the surface temperature. The experimental results have been determined by tunable vacuum ultraviolet laser ionization spectroscopy for D_2 while the theoretical results have been derived from six-dimensional quantum calculations for H_2 (after [42]).

with the surface temperature. The experimental results have been obtained by tunable vacuum ultraviolet laser ionization spectroscopy for D_2 [42]. Deuterium is often used in desorption experiments because of the unavoidable H_2 background in the vacuum chambers. The calculations, on the other hand, are done for H_2 because of the much smaller computational effort for light hydrogen in quantum methods. Still both experiment and theory agree well as far as the so-called rotational cooling is concerned, thus confirming the rotational hindering.

In Fig. 14, additionally the calculated and measured vibrational temperatures [42] are plotted. In contrast to the rotational cooling, there is vibrational heating indicating that there should be enhanced dissociation for vibrating hydrogen molecules on Pd(100). Usually vibrational enhanced dissociation is associated with strongly curved reaction paths in activated systems [43]. However, the most favorable path towards dissociative adsorption in the system H_2/Pd(100) is purely attractive and has a rather small curvature (see Fig. 8). Therefore one would not expect any substantial influence of the vibrational state of H_2 on the sticking probability.

In fact, the vibrational effects in the system H_2/Pd(100) are also present in adiabatic calculations in which the vibrational state of the molecule is kept fixed so that no vibrational transitions are allowed [44]. A detailed analysis showed that the vibrational effects in the dissociation of H_2/Pd(100) are caused by the strong lowering of the H-H vibrational frequency during the adsorption and the multidimensionality of the relevant phase space with its broad distribution of barrier heights. This can be understood from the fact that the vibrational motion corresponds to the fastest degree of freedom in this system so that the vibrational energy acts as an adiabatic invariant. The higher the vibrational energy, the stronger the effect of the lowering of the vibrational frequency. Therefore vibrationally excited molecules experience a potential energy surface with effectively lower barriers than molecules in the vibrational ground state causing vibrationally enhanced dissociation in adsorption and vibrational heating in desorption.

In fact, an earlier experiment showed a vibrational overpopulation of the first excited vibrational state in desorption that was higher than the vibrational ground-state population by a factor of nine [45]. This result was later questioned on the basis of the quantum calculations which only found an overpopulation by a factor of 2.5 [44]. When the experiments were repeated, the theoretical predictions were confirmed [42], as Fig. 14 demonstrates. This indicates that in the field of surface science theory has reached a level of reliability that makes predictions possible and allows a fruitful and close collaboration with experiment.

V. Scattering

Information about the molecule-surface interactions can not only be gained by considering adsorption or desorption, but also by studying the scattering of molecules from surfaces. Due to the reactive nature of the H_2-palladium interaction, the potential energy surface is strongly corrugated and anisotropic with regard to the molecular orientation. Since H_2 is such a light molecule, coherence effects should lead to diffraction patterns in the H_2 scattering from periodic surfaces. Because of the anisotropy of the PES, in addition to elastic diffraction peaks there should be large intensities in rotationally inelastic diffraction peaks which correspond to rotational transitions in the collision process. This is indeed the case, as the six-dimensional quantum coupled-

channel calculations for the scattering of H_2/Pd(100) have shown [46]. In this calculations, again a parametrization of the *ab initio* PES plotted in Fig. 8 has been used.

One typical calculated angular distribution of H_2 molecules scattered at Pd(100) is shown in Fig. 15. The total initial kinetic energy is E_i = 76 meV. The incident parallel momentum corresponds to 2 $\hbar$G along the $\langle 0\,\bar{1}\,1 \rangle$ direction. This leads to an incident angle of $\theta_i = 32^o$. The molecules are initially in the rotational ground state $j_i = 0$. (m, n) denotes the parallel momentum transfer $\mathbf{\Delta G}_\parallel = (mG, nG)$. The specular peak is the most pronounced one, but the first order diffraction peak (10) is only a factor of four smaller. The results for the rotationally inelastic diffraction peaks $j = 0 \rightarrow 2$ have been summed over all final azimuthal quantum numbers m_j. The excitation probability of the so-called cartwheel rotation with $m = 0$ is for all peaks approximately one order of magnitude larger than for the so-called helicopter rotation $m = j$, since the polar anisotropy of the PES is stronger than the azimuthal one.

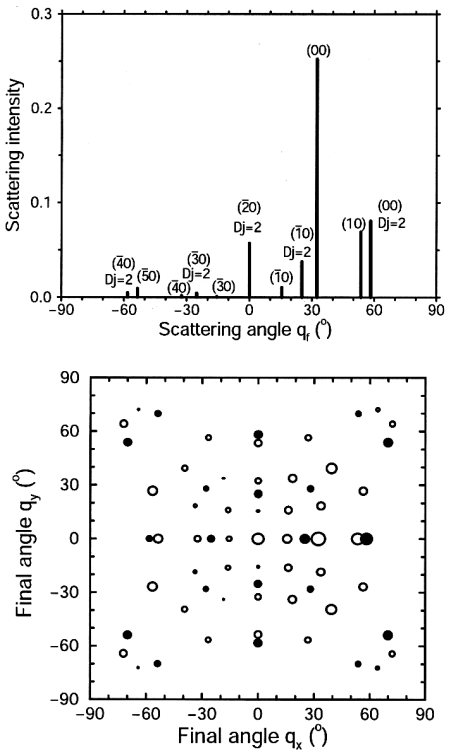

Figure 15. Six-dimensional quantum results of the rotationally inelastic scattering of H_2 molecules on Pd(100) for a kinetic energy of 76 meV at an incidence angle of 32° along the [10] direction of the square surface lattice. The upper panel shows the inplane diffraction spectrum where all peaks have been labeled according to the transition. The lower spectrum shows all diffraction peaks where the open and filled circles correspond to the rotationally elastic and rotationally inelastic scattering, respectively. The radius of the circles is proportional to the logarithm of the scattering intensity (after [46]).

This steric effect in scattering could already be expected from detailed balance arguments. According to the principle of detailed balance, in an equilibrium situation the flux impinging on a surface from the gas-phase, which is rotationally isotropically distributed, should equal the desorption plus the scattering flux. Since in desorption the helicopter rotations are preferentially occupied, the cartwheel rotations have to be preferentially excited in scattering.

The intensity of the rotationally inelastic diffraction peaks in Fig. 15 is comparable to the rotationally elastic ones. Except for the specular peak they are even larger than the corresponding rotationally elastic diffraction peak with the same momentum transfer (m, n). Note that due to the initial conditions the rotationally elastic and inelastic ($\bar{2}0$) diffraction peaks fall upon each other.

The out-of-plane scattering intensities are not negligible, which is demonstrated in the lower panel Fig. 15. The open circles correspond to rotationally elastic, the filled circles to rotationally inelastic diffraction. The radii of the circles are proportional to the logarithm of the scattering intensity. The sum of all out-of-plane scattering intensities is approximately equal to the sum of all in-plane scattering intensities. Interestingly, some diffraction peaks with a large parallel momentum transfer still show substantial intensities. This phenomenon is well known from helium atom scattering and has been discussed within the concept of so-called rainbow scattering.

The experimental observation of diffraction in reactive systems is not trivial. Because of the reactivity, an adsorbate layer builds up very rapidly during the experiment. These layers destroy the perfect periodicity of the surface and thus suppress diffraction effects. In order to keep the surface relatively clean, one has to use rather high surface temperatures so that adsorbates quickly desorb again. High surface temperatures, on the other hand, also smear out the diffraction pattern. Still experimentalists managed to clearly resolve rotationally inelastic peaks in the diffraction pattern of D_2/Ni(110) [47] and D_2/Rh(110) [48] in addition to rotationally elastic peaks.

VI. Conclusions

In this review, we have presented theoretical studies of the interaction of hydrogen atoms and molecules with palladium surfaces based on first-principles total-energy calculations. The calculations and simulations agree very favorably with experimental results. Not only quantitative agreement with experiment is achieved, but also important qualitative concepts emerge from the electronic structure calculations as well as from the high-dimensional dynamical simulations. These concepts are applicable to any reaction system. This makes hydrogen/palladium a model system of general importance whose study is not yet finished. In the future, more complex surface structures and processes will be investigated which will further deepen our understanding of the interaction of atoms and molecules with surfaces.

Acknowledgments

Financial support by the Deutsche Forschungsgemeinschaft through Sonderforschungsbereich 338 is gratefully acknowledged.

References

1. A. Dedieu, Chem. Rev. **100**, 543 (2000).
2. K. Balasubramanian, P. Y. Feng, and M. Z. Liao, J. Chem. Phys. **88**, 6955 (1988).
3. K. Balasubramanian, J. Chem. Phys. **93**, 8061 (1990).
4. S. Wilke, D. Hennig, and R. Löber, Phys. Rev. B **50**, 2548 (1994).
5. A. Roudgar and A. Groß, J. Electroanal. Chem. **548**, 121 (2003).
6. J. P. Perdew et al., Phys. Rev. B **46**, 6671 (1992).
7. W. Dong, V. Ledentu, P. Sautet, A. Eichler, and J. Hafner, Surf. Sci. **411**, 123 (1998).
8. S. Wilke and M. Scheffler, Phys. Rev. B **53**, 4926 (1996).
9. V. Ledentu, W. Dong, P. Sautet, A. Eichler, and J. Hafner, Phys. Rev. **57**, 12482 (1998).
10. M. Lischka and A. Groß, Phys. Rev. **65**, 075420 (2002).
11. U. Muschiol, P. K. Schmidt, and K. Christmann, Surf. Sci. **395**, 182 (1998).
12. A. Eichler, G. Kresse, and J. Hafner, Surf. Sci. **397**, 116 (1998).
13. A. Eichler, J. Hafner, J. Furthmüller, G. Kresse, Surf. Sci. **346**, 300 (1996).
14. B. Hammer and J. K. Nørskov, Nature **376**, 238 (1995).
15. B. Hammer and J. K. Nørskov, Surf. **343**, 211 (1995).
16. B. Hammer, Surf. Sci. **459**, 323 (2000).
17. E. Kampshoff, N. Waelchli, A. Menck, and K. Kern, Surf. Sci. **360**, 55 (1996).
18. J. Yoshinobu, H. Tanaka, and M. Kawai, Phys. Rev. B **51**, 4529 (1995).
19. D. Tománek, S. Wilke, and M. Scheffler, Phys. Rev. Lett. **79**, 1329 (1997).
20. J.-F. Paul and P. Sautet, Phys. Rev. **53**, 8015 (1996).
21. R. Löber and D. Hennig, Phys. Rev. **55**, 4761 (1997).
22. R. A. Olsen, P. H. T. Philipsen, E. Baerends, G. J. Kroes, and O. M. Løvvik, J. Chem. Phys. **106**, 9286 (1997).
23. R. A. Olsen, G. J. Kroes, O. M. Løvvik, and E. J. Baerends, J. Chem. Phys. **107**, 10652 (1997).
24. G. E. Gdowski, R. H. Stulen, and T. Felter, J. Vac. Sci. Technol. A **5**, 1103 (1987).
25. K. Christmann, Surf. Sci. Rep. **9**, 1 (1988).
26. W. Dong and J. Hafner, Phys. Rev. B **56**, 15396 (1997).
27. V. Ledentu, W. Dong, and P. Sautet, Surf. Sci. **412**, 518 (1998).
28. C. M. Wei, A. Groß, and M. Scheffler, Phys. Rev. B **57**, 15572 (1998).
29. K. D. Rendulic, G. Anger, and A. Winkler, Surf. Sci. **208**, 404 (1989).
30. M. L. Burke and R. J. Madix, Surf. Sci. **237**, 1 (1990).
31. S. Wilke and M. Scheffler, Phys. Rev. Lett. **76**, 3380 (1996).
32. P. Avouris, D. Schmeisser, and J. E. Demuth, Phys. Rev. Lett. **48**, 199 (1982).
33. S. Andersson and J. Harris, Phys. Rev. Lett. **48**, 545 (1982).
34. P. K. Schmidt et al., Phys. Rev. Lett. **87**, 096103 (2001).
35. A. Gross, S. Wilke, and M. Scheffler, Phys. Rev. Lett. **75**, 2718 (1995).
36. A. Eichler, J. Hafner, A. Groß, and M. Scheffler, Phys. Rev. B **59**, 13297 (1999).
37. K. D. Rendulic and A. Winkler, Surf. Sci. **299/300**, 261 (1994).
38. D. A. King, CRC Crit. Rev. Solid State Mater. Sci. **7**, 167 (1978).
39. A. Gross, S. Wilke, and M. Scheffler, Surf. Sci. **357/358**, 614 (1996).
40. M. Beutl, M. Riedler, and K. D. K.D. Rendulic, Chem. Phys. Lett. **247**, 249 (1995).
41. M. Gostein and G. O. Sitz, J. Chem. Phys. **106**, 7378 (1997).
42. D. Wetzig, M. Rutkowski, H. Zacharias, and A. Groß, Phys. Rev. B **63**, 205412 (2001).
43. G. R. Darling and S. Holloway, Rep. Prog. Phys. **58**, 1595 (1995).
44. A. Gross and M. Scheffler, Chem. Phys. Lett. **256**, 417 (1996).
45. L. Schröter, H. Zacharias, and R. David, Phys. Rev. Lett. **62**, 571 (1989).
46. A. Gross and M. Scheffler, Chem. Phys. Lett. **263**, 567 (1996).
47. M. F. Bertino, F. Hofmann, and J. P. Toennies, J. Chem. Phys. **106**, 4327 (1997).
48. D. Cvetko, A. Morgante, A. Santaniello, and F. Tommasini, J. Chem. Phys. **104**, 7778 (1996).